encit 2020

ABCM Associação Brasileira de Engenharia e Ciências Mecânicas

18th Brazilian Congress of Thermal Sciences and Engineering
November 16–20, 2020 (Online)

ENC-2020-0673
EXPERIMENTAL CHARACTERIZATION OF THE FLOW STRUCTURE IN ACCELERATED BUBBLY FLOWS ENCIT 2020

Andreza Sousa Ribeiro
Rafael Franklin Lázaro De Cerqueira
Emilio Ernesto Paladino
SINMEC - Computational Fluid Dynamics Lab, Department of Mechanical Engineering, Federal University of Santa Catarina, Florianopolis, SC, 88040-900, Brazil
andreza.ribeiro@sinmec.ufsc.br
rafaelfc@sinmec.ufsc.br
paladino@sinmec.ufsc.br

Abstract. *Accelerated bubbly flows have a broad application in various engineering fields. Several authors analyzed the flow and turbulence structure in vertical bubbly pipe flows. However, only a few studies focused on the flow structure in accelerated flows as encountered in flow constrictions, as contractions or bends, specially using the PIV technique which allows for the measurement of the detail of the flow structure. In this work, the flow structure in accelerated vertical air-water flows through convergent-divergent duct was investigated. The liquid phase velocity was measured by the Particle Image Velocimetry technique, using fluorescent tracer particles (PIV/LIF). A Particle Tracking Velocimetry (PTV) technique was used to obtain the bubble size and velocity distribution. In order to overcome the issues related to the presence of bubbles in the PIV measurements of the liquid phase velocity, a technique was employed to remove the dispersed gas phase contribution in the averaged liquid velocity results. The PIV and the PTV methods were validated through a series of gas-liquid vertical bubbly at the inlet section, confirming the reliability of the experimental techniques. The results for the liquid velocity fields in convergent-divergent duct show that the flow structure in completely modified by the presence ob bubbles, even in very low volume fractions, specially, for low liquid superficial velocities.*

Keywords: *Accelerated Flow, Bubbly Flow, PIV, PTV*

1. INTRODUCTION

Gas-liquid bubbly flows are important in different fields of engineering, such as energy conversion system including nuclear power plants, petro-chemical plants and metallurgical equipment (Serizawa and Kataoka, 1990).

In general, studies on air-water bubbly flow are common in pipes. Sato and Sekoguchi (1975) presented a theoretical relationship between liquid velocity and void fraction. A proposal was offered for introducing an additional shear stress due to bubble motion. Also, comparisons were made between the predictions and measurements on vertical upward air-water bubble flow.

In the work of Fujiwara *et al.* (2004), the authors studied the structure of turbulence modification in terms of bubble diameter in a fully developed pipe flow. The authors deduced a correlation between the global turbulence flow structure and the local turbulence modification induced by the presence of bubbles and as characterized by the instantaneous vorticity from experimental results, obtained by the PIV/LIF technique.

On of the first studies of gas-liquid bubbly flows in a Venturi tube, wer presented by Thang and Davis (1979). In that work the authors determined the local distribution of the flow structure parameters, such as void fraction, bubble frequency and velocity, bubble size and the average velocity ratio between the gas and the liquid phases at characteristic locations along a Venturi. However, the technique used allowed only for teh local measurement of the bubbles velocities and no information about the local velocity distribution of the liquid phase was presented.

Recent works on bubbly flow in Venturi tubes focus on type bubble generator, focusing on the analysis of the bubble breakage. Zhao *et al.* (2018) investigated the movement and breakup of individual bubbles in a Venturi channel with a rectangular cross section for better observation. The motion of bubbles and their interaction with liquid were recorded by a high speed camera, from which relevant parameters including bubble size, trajectory and velocity were obtained by a Digital Image Analysis (DIA) method.

Huang *et al.* (2019) studied experimentally the performance of a micro-scale Venturi channel as a bubble generator to explore its potential regarding the producing of micro-bubbles. Moreover, the flow patterns in the diverging section were

investigated owing to their significance for the mechanisms dominating the bubble breakups.

In Song *et al.* (2019), the authors analyzed the bubble breakup mechanism in a Venturi bubble generator. High-speed imaging was used to analyze the motion, deformation and break-up of the bubbles. However, the PIV technique is only applied for the analysis of single phase liquid flow, in order to measure the turbulent fields and relate them with bubble break-up.

According to the authors knowledge, there are no studies in the literature analyzing the flow structure of the liquid phase in air-water bubbly flows in convergent-divergent sections. Hence, the main objective of the present work is to analyze the effect of the dispersed bubbles on the flow structure in gas-liquid bubbly flows in convergent divergent section. These result are also useful for the validation of CFD model in accelerated bubbly flows.

2. METHODOLOGY

2.1 Experimental Setup

Figure 1 shows schematically the experimental apparatus. The transparent acrylic test section is interchangeable, where was placed a convergent-divergent section. The section, positioned before the test section, is made of a transparent acrylic and has a length of about $L = 2$ m, resulting in a length of 50 diameter before the measurement section.

The water flow rate is measured by two OMEGA FL46303/SED Flow Control flow meters with ranges of 1.00-7.50 l/min and 60-600 l/h, both with $\pm 5.0\%$ full-scale. The liquid phase flow rate is controlled by a frequency inverter connected to the electric water pump motor.

The dispersed bubbles are injected at the bottom of the tube through a porous gas diffuser, in order to control the sizes of the dispersed bubbles. The gas flow rate is controlled by a needle valve and measured by an OMEGA FL-3802ST/FL-3861SA flow meter with range of 81.4-814.0 standard mL/min, with $\pm 2.0\%$ full-scale accuracy.

A box constructed with transparent acrylic made with 8 plane faces at the PIV measurement section, filled with the same liquid as in the pipe in order to minimize the optical distortion.

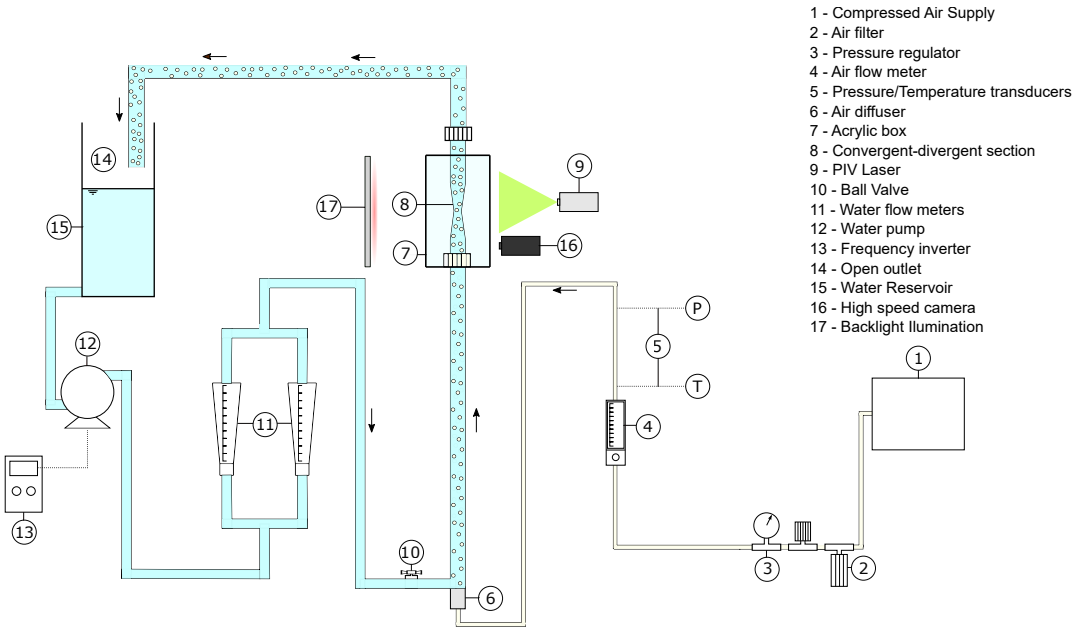

Figure 1: Schematic of the experimental setup. Adapted from Cerqueira *et al.* (2018)

Figure 2 a photograph of the convergent-divergent section. The section is constructed with transparent acrylic and consists of three portions, which are the divergent segment (DS), the throat segment (TS) and the convergent segment (CS). The ratio of internal throat diameter to the internal upstream pipe diameter is 0.2. The internal diameter of the section is 44 mm and the wall thickness is 3 mm. The angles of the convergent and divergent section are 20 degrees.

2.2 PIV/LIF Phase

The standard PIV technique was largely described in the literature (e.g., Raffel *et al.* (2007)) and, therefore, will no be described here. The PIV system available at SINMEC Lab consists of a TSI 9 MPx resolution CCD camera, a pulsed Nd:YAG laser with a wavelength of 532 nm and a synchronizer to match the emission of laser pulses and image capturing In applications to gas-liquid two-phase flows, the presence of the interfaces scatters the light of the laser with much more

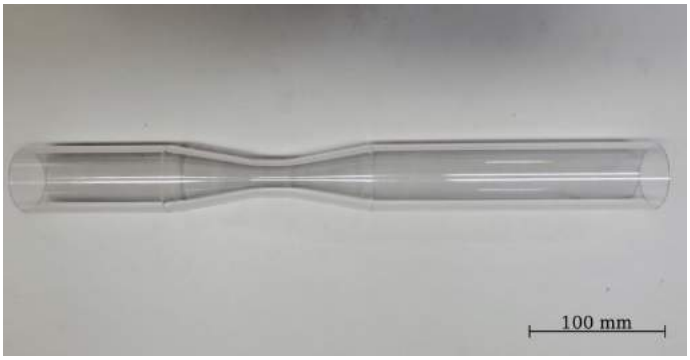

Figure 2: Photograph of the convergent-divergent section.

intensity than these particles, impeding the CCD camera to capture the seeding particles. Therefore, the LIF technique was employed, using fluorescent seeding particles and an optical filter in front of the camera lens. Particles of Rhodamine B, with diameters ranging from 1 to 20 lm were used, which receive light in a wavelength of 532 nm and emit (fluorescence) at 590 nm (peak). A high band-pass filter for the wavelengths above 545 nm is used at the camera lens, filtering all the light at the laser wavelength (scattered by the interfaces) and capturing the light fluoresced by the seeding particles. In this way, only the fluorescent particles, seeded into the liquid phase are, *a priori*, captured in the images. However, the fluoresced light emitted by these particles can be also reflected by the interfaces leading to a biasing in the measurement of liquid velocity. Therefore, a discrimination technique presented in Cerqueira *et al.* (2018), and summarized in the next section, was used to avoid this biasing.

2.3 Phase discrimination algorithm

According to Cerqueira *et al.* (2018), the PIV technique produces unacceptable vectors in interrogation windows occupied by bubbles, which lead to biasing in the ensemble average results. This sort of error can introduce some bias in the velocity fields, since the seeded particles, which are only present in the liquid phase, appear to be in the gas phase due to the reflection of fluoresced light on interfaces and off-plane particles illuminated by scattered light. Those unrealistic velocity vectors in the time averaging procedure overestimates the liquid velocity averaged fields due to the higher velocity of the bubbles.

The phase discrimination algorithm developed by authors, is used this work to remove these unrealistic velocity vectors, by analyzing the PIV/LIF raw images. This algorithm identify the interrogation windows occupied by bubbles and remove its contribution for the ensemble average of liquid velocity.

2.4 PTV for bubble tracking

The PTV (Particle Tracking Velocimetry) method is based on backlight illuminated footage, is used for obtain information about gas phase such as velocity, bubble size and shape. Furthermore, it is used also to verify the liquid velocity fields obtained from the PIV/LIF method. The details of the image processing and application of PTV can be encountered in Cerqueira *et al.* (2018) and Cerqueira and Paladino (2021). This verification is performed as discussed in Cerqueira *et al.* (2018), by comparing the average liquid velocity obtained by the PIV and that calculated indirectly from the gas volume fraction, which is calculated fro the average bubble velocity obtained from the PTV technique,.

3. RESULTS AND DISCUSSION

3.1 Experimental matrix

Table 1 shows the experimental matrix, where the liquid j_l and gas j_g superficial velocities were calculated based on the gas and liquid flow rate mesurents on inlet section. The gas volume fraction $\langle \alpha_g^{in\cdot} \rangle$ was calculated using the bubble tracking method (PTV) described in Section 2.4 as,

$$\langle \alpha_g^{in\cdot} \rangle = \frac{Q_g}{A_{duct}} \frac{1}{\overline{\langle v_g \rangle}} \tag{1}$$

where Q_g is the gas flow rate measured by the rotameter and $\overline{\langle v_g \rangle}$ is the average gas pahse velocity obtained fro the PTV technique.

In this work, two single-phase flow conditions and 6 two-phase flow conditions are going to tested. Note the differences between j_g values from laminar and turbulent flow. High values of j_g in laminar flow cause many bubbles on flow, turns

the PIV and PTV measurement impossible.

Table 1: Test matrix of the experiements.

Case	j_l [m/s]	j_g [m/s]	$\langle \alpha_g^{in.} \rangle$ [-]
1	$10.96 \cdot 10^{-3}$	0.0	-
2		$1.00 \cdot 10^{-3}$	0.005
3		$1.50 \cdot 10^{-3}$	0.008
4		$2.05 \cdot 10^{-3}$	0.011
5	$131.53 \cdot 10^{-3}$	$0.0 \cdot 10^{-3}$	-
6		$2.05 \cdot 10^{-3}$	0.006
7		$4.05 \cdot 10^{-3}$	0.012
8		$5.97 \cdot 10^{-3}$	0.018

3.2 Techniques validation

The experimental technique used for the measurement of liquid phase velocity, in particular, the method for phase discrimination, are validated following the procedure given in Cerqueira *et al.* (2018).

In order to validate the calibration of the PIV system, the liquid flow rate calculated from the PIV $\left(Q_l^{PIV}\right)$ Eq.(2) is compared with liquid rotameter flow rate $\left(Q_l^{Rot}\right)$,

$$\overline{\langle v_l \rangle} = \frac{Q_g}{A_{duct} \cdot \langle \alpha_l \rangle} = \frac{2}{R^2} \cdot \sum_{i=1}^{I} \left[\langle v_{l,i}(r_i) \rangle \cdot r_i \cdot \Delta r_i \right] \tag{2}$$

where Q_g is the volumetric gas flow rate, A_{duct} e R is the transverse area and radius of the inlet section, respectively and the index i represent the radial direction divided by I interrogation windows.

Table 2 presents the comparison of the liquid flow rate measured by $\left(Q_l^{Rot}\right)$ and the numerically integrated $\left(Q_l^{PIV}\right)$ value from the PIV liquid velocity profiles in inlet section. The results show that the deviation between the two values is within the range of the liquid rotameter accuracy ($\pm 5.0\%$ full scale).

Table 2: Comparision between the liquid flow rate from PIV and values read from the liquid rotameter in inlet section.

Re_l	$Q_l^{Rot.}$ [m^3/s]	Q_l^{PIV} [m^3/s]	Deviation [%]
482	$1.66 \cdot 10^{-5}$	$1.64 \cdot 10^{-5}$	1.14%
5787	$2.0 \cdot 10^{-4}$	$2.01 \cdot 10^{-4}$	0.79%

Figure 3 shows different liquid axial velocity profiles $\overline{\langle v_l(r,z) \rangle}$ for cases shows in Tab. 1. The results with phase discrimination algorithm (right) resulted in lower upward axial velocities when compared to results without this algorithm (left).

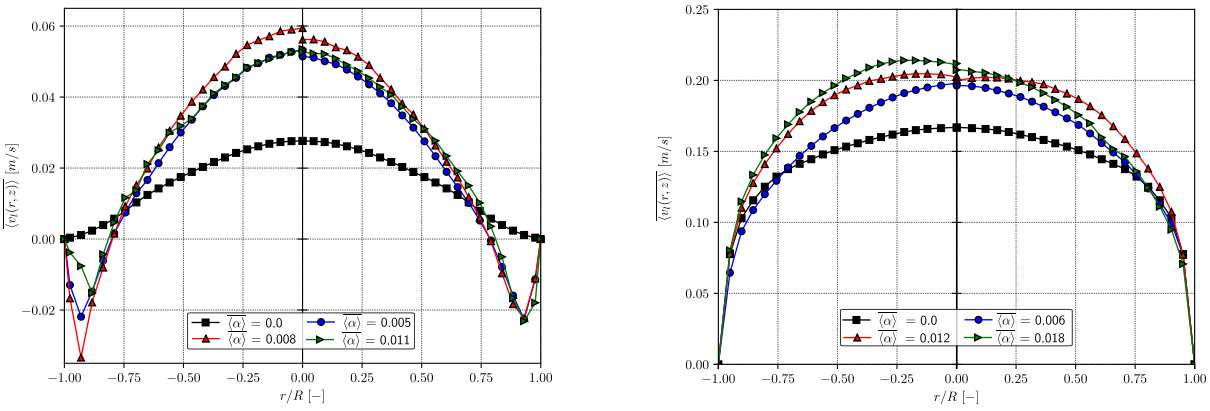

(a) (b)

Figure 3: Average liquid axial velocity profiles on inlet section. The velocity profiles on the left represent the results without the phase discrimination algorithm and the right are obtained after the phase dicrimination algorithm: (a) Cases 1, 2, 3 and 4 and (b) Cases 5, 6, 7 and 8 in Table 1.

The validation is done by comparing the values of $\overline{\langle v_l^*(r,z)\rangle}$ (calculated through Eq. 3), obtained review from the PTV tecnhique, following the procedure given in (Cerqueira *et al.*, 2018).

$$\overline{\langle v_l^*(r,z)\rangle} = \frac{\overline{\langle j_l \rangle}}{1 - \overline{\langle \alpha_g \rangle}} \tag{3}$$

Table 3 shows the comparision of the $\overline{\langle v_l^*(r,z)\rangle}$ values from Eq. (3) and PIV results. It can be observed the results from both methods present excellent agreement, showing that the phase discrimination algorithm and PTV for bubble tracking technique used in this work originates reliable results.

Table 3: Comparision between the $\overline{\langle v_l^*(r,z)\rangle}$ values from Eq. (3) and PIV results.

Case	$\overline{\langle v_l^*(r,z)\rangle}$ [m/s]	$\overline{\langle v_l(r,z)\rangle}$ [m/s]	Deviation [%]
2	$11.25 \cdot 10^{-3}$	$11.02 \cdot 10^{-3}$	2.09%
3	$11.63 \cdot 10^{-3}$	$11.05 \cdot 10^{-3}$	5.25%
4	$11.95 \cdot 10^{-3}$	$11.09 \cdot 10^{-3}$	7.75%
6	$138.70 \cdot 10^{-4}$	$132.40 \cdot 10^{-3}$	4.76%
7	$139.33 \cdot 10^{-4}$	$133.21 \cdot 10^{-3}$	4.59%
8	$139.71 \cdot 10^{-4}$	$134.07 \cdot 10^{-3}$	4.21%

As can be observed, results for inlet section present good agreement. Therefore, PIV/LIF phase, PTV for bubble tracking and phase discrimination algorithm can be considered reliable for PIV measurements.

3.3 Analisys of the flow structure

The results will focus on the local analysis of the average liquid velocity and fluctuations in convergent-divergent section, such as radial profiles along the middle plane of the domain. By analysing those results, it is possible to understand how the dispersed bubbles modify the flow structure of the liquid phase in the convergent-divergent section.

Figure 4 shows liquid axial velocity distribuition for j_l = 10,96 $\cdot$ 10^{-3} m/s and different gas supercial velocities.

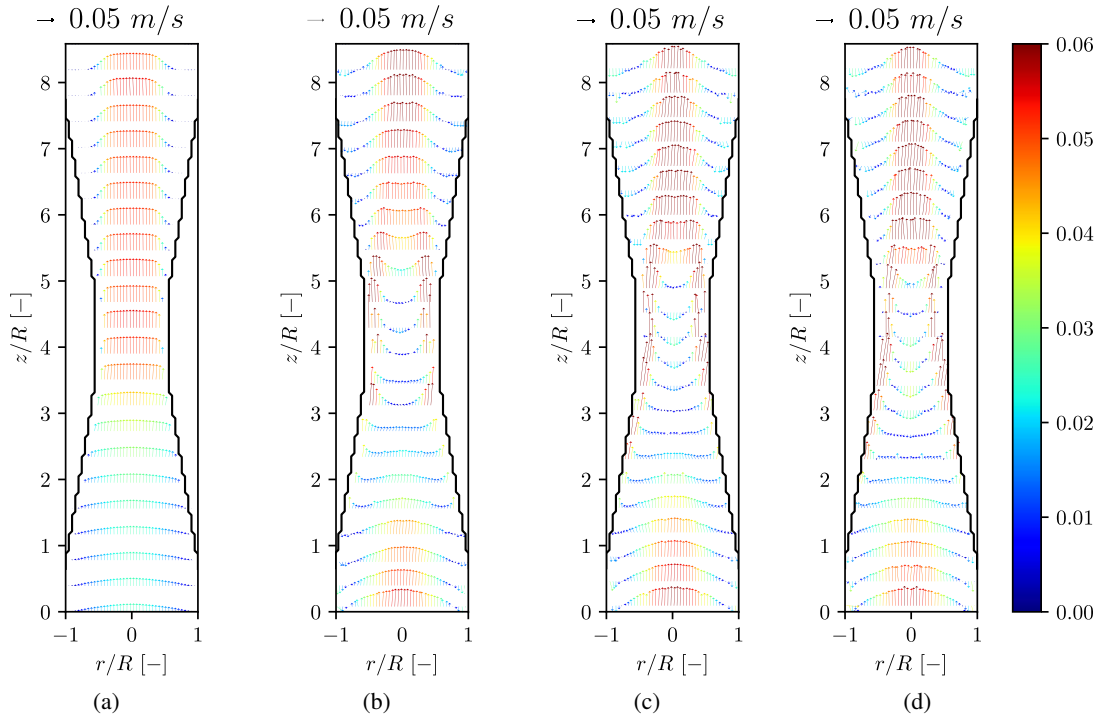

Figure 4: Liquid velocity axial distribution for j_l = 10,96 $\cdot$ 10^{-3} m/s for different gas superficial velocities: (a) j_g = 0,0 m/s, (b) j_g = 1,00 $\cdot$ 10^{-3} m/s, (c) j_g = 1,50 $\cdot$ 10^{-3} m/s and (d) j_g = 2,05 $\cdot$ 10^{-3} m/s.

It can be observed that the presence of the bubbles in the flow affects the liquid profiles significantly. For cases with lower liquid superficial velocity, at the inlet region, the velocity profiles tends to form a "pike" in the core region which

descreases towards the wall, indicating the presence of a downward liquid film, induced by liquid dragged by gas bubbles in the core region, which is more evident in higher gas void fractions. This downward liquid as also been observed in mean axial velocity of duct in Cerqueira *et al.* (2018).

In the convergent section, this downward velocity near wall becomes less intense and when arrive the throat, the opposite happens: liquid negatives velocities on core and upward peaks near the wall. The maximum liquid velocities near the wall could indicate the presence of bubbles in this region, despite not having measured the void fraction radial distribution.

In the divergent section, there are two regions of liquid recirculation pronounced and intense. The maximum velocity occurs in the central region.

Figure 5 shows liquid axial velocity distribuition for j_l = 131,53 · 10^{-3} m/s and different gas supercial velocities.

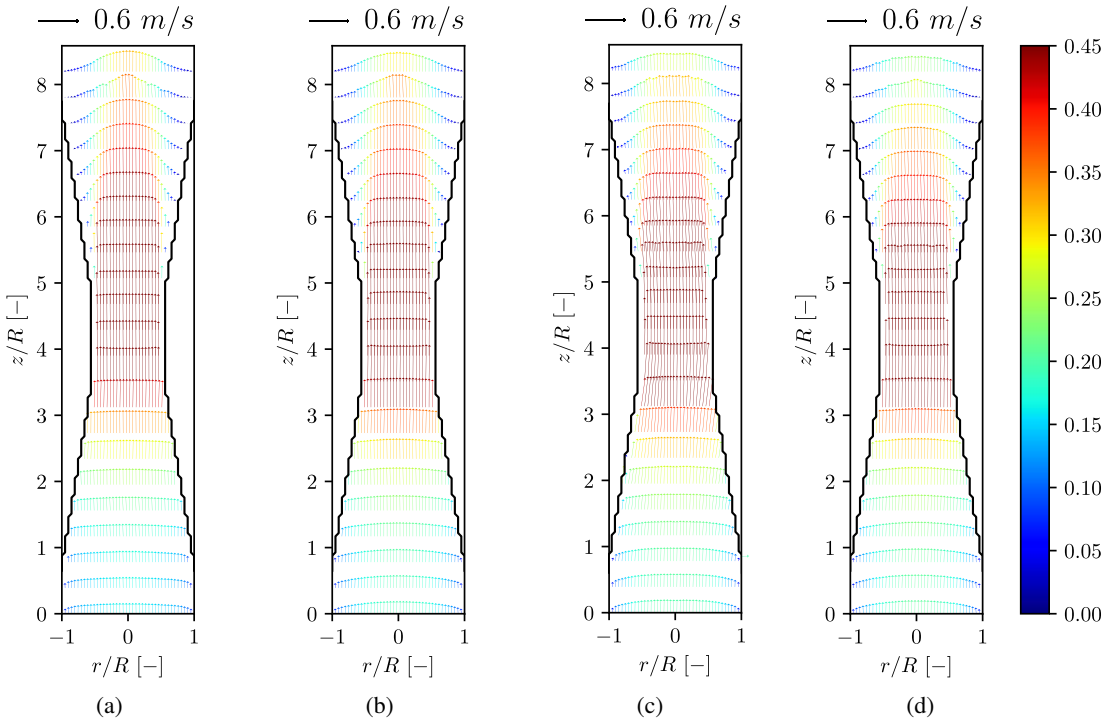

Figure 5: Liquid velocity axial distribution for j_l = 131,53 · 10^{-3} m/s for different gas superficial velocities: (a) j_g = 0,0 m/s, (b) j_g = 2,05 · 10^{-3} m/s, (c) j_g = 4,05 · 10^{-3} m/s and (d) j_g = 5,97 · 10^{-3} m/s.

For the cases with higher superficial liquid velocity the liquid velocities profiles are also affected byu te dispersed bubbles, however, keepon a similar flow structure to the single-phae case, opposit to whta is observed for the lower value of j_l. The velocity liquid profiles In the inlet region follow the same trend found in Liu and Bankoff (1993), but in a duct, where the velocity profile changes from flat in the single-phase case to convex as the void fraction increased, with a following increase of the liquid velocity in the core region.

At the test section, there is an increase in the liquid velocity in all the radial direction, indicating that the gas flow, in other words, the amount of bubbles is sufficient to occupy the entire diameter along the test section and in the divergent region, as opposed happens in the case of lower liquid superficial, the continuous phase has no moment enough to form regions of liquid recirculation.

Figure 6 shows liquid axial fluctuation velocity distribuition for j_l = 10,96 · 10^{-3} m/s and different gas supercial velocities.

The results presented in the Figures 6 show that a small quantity of bubbles in the flow results in a significant increase turbulent fluctuations in the liquid phase.

Until the z/R = 2, turbulence in the central region increased strongly with the increase of void fraction. That same effect was observed by Liu and Bankoff (1993), in a duct of constant section, in which bubble-induced turbulence is more pronounced in the core region.

At z/R = 5, although bubbles not concentrated near wall, the maximum of turbulent fluctuations occurs in this region. Such phenomenon happens because the liquid recirculations at the divergent section result in a region of pronounced shear, increasing the production of turbulent kinetic energy.

According to Hosokawa and Tomiyama (2013), the bubble induced turbulence (BIT) exists even where the bubble concentration is very small. This is because the diffusion of turbulent kinetic energy occurs from a high to low void

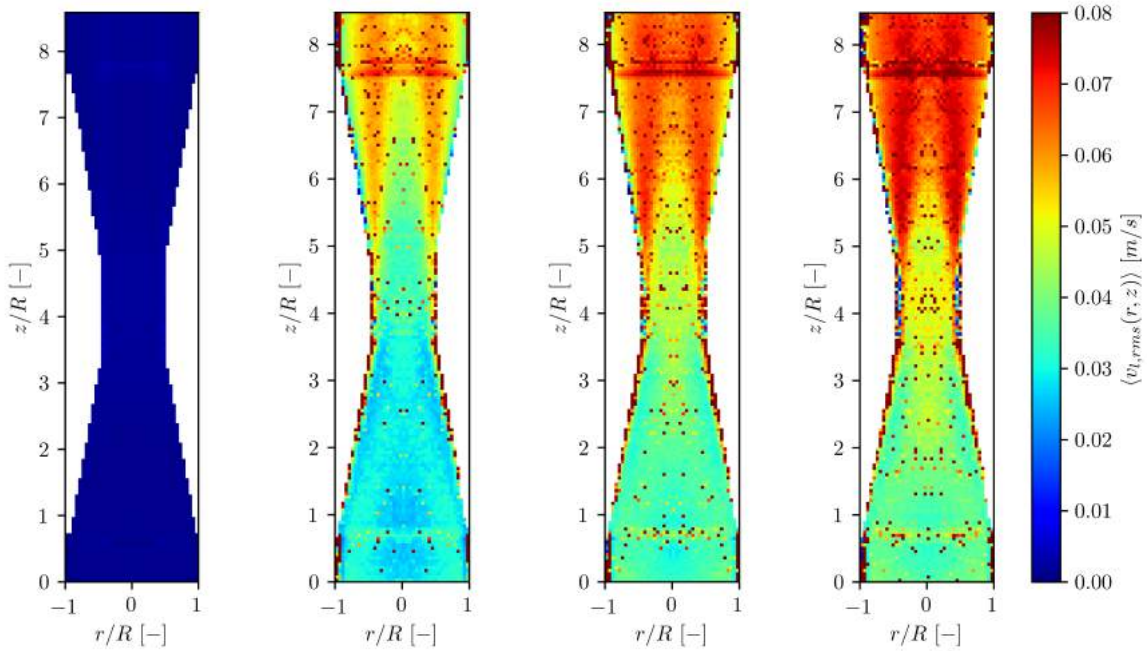

(a) (b) (c) (d)

Figure 6: Liquid axial velocity fluctuation distribution distribution for j_l = 10,96 · 10^{-3} m/s for different gas superficial velocities: (a) j_g = 0,0 m/s, (b) j_g = 1,00 · 10^{-3} m/s, (c) j_g = 1,50 · 10^{-3} m/s and (d) j_g = 2,05 · 10^{-3} m/s.

fraction region.

Figure 7 shows liquid axial fluctuation velocity distribuition for j_l = 131,53 · 10^{-3} m/s and different gas supercial velocities.

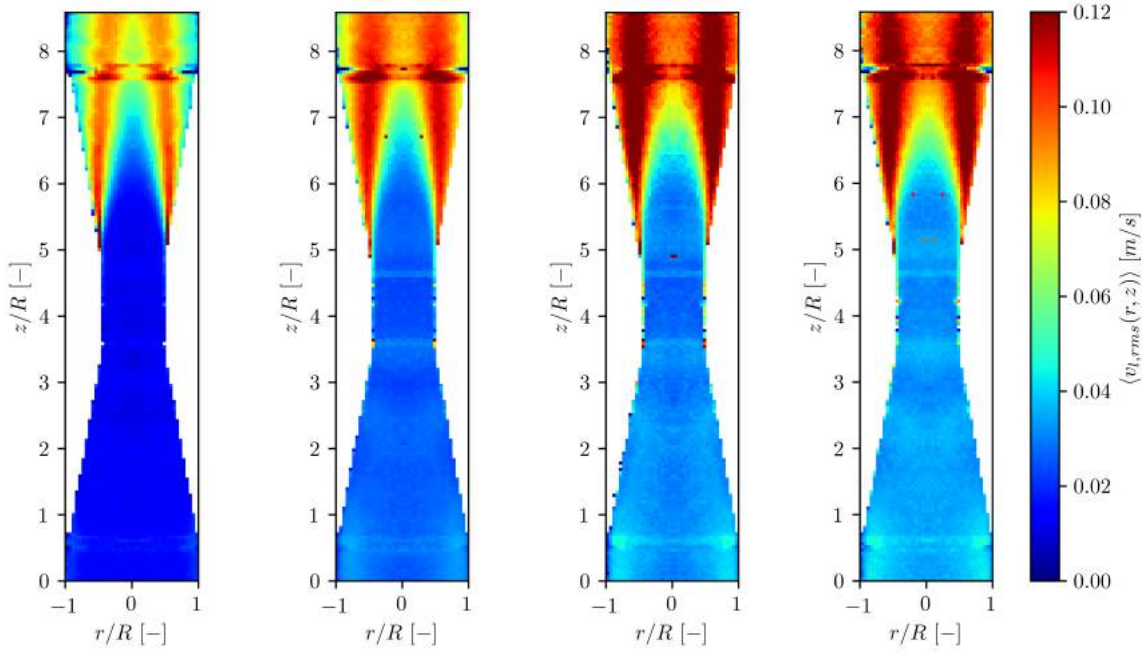

(a) (b) (c) (d)

Figure 7: Liquid axial velocity fluctuation distribution for j_l = 131,53 · 10^{-3} m/s for different gas superficial velocities: (a) j_g = 0,0 m/s, (b) j_g = 2,05 · 10^{-3} m/s, (c) j_g = 4,05 · 10^{-3} m/s and (d) j_g = 5,97 · 10^{-3} m/s.

From Figures 7, the presence of the dispersed bubbles promotes a relative uniforme turbulence distibution, indicanting that the gas bubbles promores a stroges radial momentum tranfer. (Liu and Bankoff, 1993)

4. CONCLUSIONS

In this work, the bubbly flow structure in a convergent-divergent pipe section, for different superficial velocities of gas and liquid was studied. The study of the two-dimensional flow structure of the liquid phase in constrictions and/or sections variation of diameter was little studied in literature. In general, the studies found until now, focused on the dispersed phase, and, in particular, on the break-up and coalesce processes of bubbles.

For this purpose, two measurement techniques were used. The liquid phase was measured using the Particle Image Velocimetry technique, using fluorescent seeding particles. To overcome the problems caused by the presence of bubbles in the results PIV/LIF, a technique was used to remove the contribution from the dispersed phase in the average liquid velocities results. Particle Tracking Velocimetry was used to obtain the velocity distribution of the disperses bubbles.

The presence of dispersed bubbles, even in very low concentration, changes dramatically the flow structure, for low liquid superficial velocities, with the appearance of downward flow region in the core of the convergent section.

For the cases where the liquid flow is laminar, the presence of dispersed bubbles generates a bubble induced turbulence (BIT) in the whole test section. In the case of turbulent liquid flow, the increase of the gas volume fraction changes the turbulence, which results as the sum of BIT and the liquid phase shear induced turbulence.

5. ACKNOWLEDGEMENTS

This work was supported by CAPES, Coordenação de Aperfeiçoamento de Pessoal de Nivel Superior and Petrobras – Brazil.

6. REFERENCES

Cerqueira, R.F. and Paladino, E.E., 2021. "Development of a deep learning-based image processing technique for bubble pattern recognition and shape reconstruction in dense bubbly flows". *Chemical Engineering Science*, Vol. 230, p. 116163. ISSN 0009-2509. doi:https://doi.org/10.1016/j.ces.2020.116163. URL `http://www.sciencedirect.com/science/article/pii/S0009250920306953`.

Cerqueira, R., Paladino, E., Ynumaru, B. and Maliska, C., 2018. "Image processing techniques for the measurement of two-phase bubbly pipe flows using particle image and tracking velocimetry (piv/ptv)". *Chemical Engineering Science*, Vol. 189, pp. 1–23.

Fujiwara, A., Minato, D. and Hishida, K., 2004. "Effect of bubble diameter on modification of turbulence in an upward pipe flow". *International Journal of Heat and Fluid Flow*, Vol. 25, No. 3, pp. 481–488.

Hosokawa, S. and Tomiyama, A., 2013. "Bubble-induced pseudo turbulence in laminar pipe flows". *International Journal of Heat and Fluid Flow*, Vol. 40, pp. 97–105.

Huang, J., Sun, L., Du, M., Liang, Z., Mo, Z., Tang, J. and Xie, G., 2019. "An investigation on the performance of a micro-scale venturi bubble generator". *Chemical Engineering Journal*.

Liu, T. and Bankoff, S., 1993. "Structure of air-water bubbly flow in a vertical pipe—i. liquid mean velocity and turbulence measurements". *International Journal of Heat and Mass Transfer*, Vol. 36, No. 4, pp. 1049–1060.

Raffel, M., Willert, C.E., Wereley, S.T. and Kompenhans, J., 2007. *Particle Image Velocimetry*. 1. ISBN 9783540723073. doi:10.1007/978-3-540-72308-0.

Sato, Y. and Sekoguchi, K., 1975. "Liquid velocity distribution in two-phase bubble flow". *International Journal of Multiphase Flow*, Vol. 2, No. 1, pp. 79–95.

Serizawa, A. and Kataoka, I., 1990. "Turbulence suppression in bubbly two-phase flow". *Nuclear Engineering and Design*, Vol. 122, No. 1-3, pp. 1–16.

Song, Y., Wang, D., Yin, J., Li, J. and Cai, K., 2019. "Experimental studies on bubble breakup mechanism in a venturi bubble generator". *Annals of Nuclear Energy*, Vol. 130, pp. 259–270.

Thang, N. and Davis, M., 1979. "The structure of bubbly flow through venturis". *International Journal of Multiphase Flow*, Vol. 5, No. 1, pp. 17–37.

Zhao, L., Sun, L., Mo, Z., Tang, J., Hu, L. and Bao, J., 2018. "An investigation on bubble motion in liquid flowing through a rectangular venturi channel". *Experimental Thermal and Fluid Science*, Vol. 97, pp. 48–58.

7. RESPONSIBILITY NOTICE

The authors are solely responsible for the printed material included in this paper.